KINETICS AND MORPHOLOGICAL EVOLUTION DURING MELT CRYSTALLISATION OF MOULD FLUXES

Jung-Wook CHO

Graduate Institute of Ferrous Technology, Pohang University of Science and Technology (POSTECH), Pohang 36763, Republic of Korea

jungwook@postech.ac.kr

Introduction

Various metallurgical slags will be crystallised during a cooling process after the operation. Therefore, for better valorisation of the slags, it is essential to understand the kinetics and morphological evolution of crystallisation from the molten glassy phase. In this study, the effects of basicity (CaO/SiO_2) and other components such as B_2O_3 and Li_2O on the melt crystallisation behaviours of cuspidine ($Ca_4Si_2O_7F_2$) have been investigated under non-isothermal and isothermal conditions using a differential scanning calorimetry (DSC), which could be applied to various slag system such as tundish powder, mould flux, and electro slag re-melting slag. For analysis of the non-isothermal melt crystallisation kinetics of cuspidine in CaO-SiO_2-CaF_2-based slag system, the Matusita analysis is critically assessed to find that it is not suitable to depict non-isothermal melt crystallisation of glasses. Instead, the effective activation energy for non-isothermal crystallisation was estimated using differential iso-conversional method of Friedman analysis. Also, the investigation was carried out to understand how to control crystal morphology of CaO-SiO_2-CaF_2-based slag system. A thermodynamic method was introduced to estimate Jackson α factor of a crystal in multi-component slag system, and the parameters were calculated with the help of thermodynamic database, FactSage. Furthermore, the combined effects of Jackson α factor, undercooling and flux composition on crystal morphology in slags were discussed.

Theory to evaluate melt crystallisation kinetics

Various models have been developed to estimate the activation energy associated with the non-isothermal crystallisation from thermal analysis data, including Kissinger equation[1], Ozawa equation[2], modified Ozawa-Chen equation[3], and Matusita equations[4,5]. Among these models, Kissinger equation[1] and Matusita equations[4,5] are the most widely used approaches to determine the activation energy for the crystallisation that occurs on heating[6-10]. Moreover, they are applied frequently for the non-isothermal crystallisation of polymer melts[11–15] and metallurgical slags[16,17] that occurs on cooling.

Matusita *et al.*[5] derived a generalised expression called Matusita equation to estimate the activation energy for crystal growth

$$\ln\left[-\ln(1-x)\right] = -n\ln\beta - 1.052\frac{mE}{RT} + \text{constant} \quad (1)$$

where β is the heating rate, E is the activation energy for crystal growth, R is the ideal gas constant, x is the volume fraction of crystallised phase at a given temperature T, n and m are the numerical factors that depend on the crystallisation mechanism and summarised in Matusita[18]. Since the crystallisation mechanism is involved in Matusita equation, this model has been widely used to determine the activation energy for crystal growth. It should be stressed that both the Matusita equation was originally derived from the expressions for the crystallisation that occurs on heating. However, many practical processes of non-isothermal crystallisation proceed on cooling such as mould fluxes in continuous casting of steel. Therefore, it is highly needed to ascertain that whether the Matusita equation is applicable in estimating the activation energy for melts crystallisation.

Matusita equation was derived from the basic equation of crystal growth rate[19]

$$U = \frac{dr}{dt} = \beta\frac{dr}{dT} = U_0\exp(-E/RT)\left[1-\exp(-\Delta G/RT)\right] \quad (2)$$

where U0 is the pre-exponential factor, ΔG is the crystallisation free energy, r is the radius of a crystal particle. In case the temperature is much larger than that of maximum growth rate in the heating process, the temperature dependence of the term $1-\exp(-\Delta G/RT)$ is negligibly small compared with that of the term $\exp(-E/RT)$. Thus, Equation (2) can be rewritten as

$$U = U_0\exp(-E/RT) \quad (3)$$

During the heating of a glass from room temperature T_r to a certain temperature T, the nucleation and crystal growth will occur successively. The radius r of crystal particle can be calculated by substituting Equation (3) into Equation (2).

$$r = \int_{T_r}^{T}\frac{U}{\beta}dT = \frac{U_0}{\beta}\left[\int_0^T\exp(-E/RT)dT - \int_0^{T_r}\exp(-E/RT)dT\right] \quad (4)$$

Since the upper limit of the integral $\int_0^{T_r}\exp(-E/RT)dT$ in Equation (4) is much smaller than that of $\int_0^T\exp(-E/RT)dT$ during glass crystallisation, the term $\int_0^{T_r}\exp(-E/RT)dT$ should be negligibly small compared with the term $\int_0^T\exp(-E/RT)dT$. Therefore, Equation (4) can be simplified as follows.

$$r = \frac{U_0}{\beta}\int_0^T\exp(-E/RT)dT \quad (5)$$

Matusita[5] applied a closer approximation by employing Doyle's p-function[19] to integrate the term $\int_0^T \exp(-E/RT)\,dT$ in Equation (5). As a consequence, Equation (5) can be approximated to Equation (6)

$$r = \frac{U_0 E}{\beta R} \exp\left(-5.330 - 1.052\frac{E}{RT}\right) \tag{6}$$

When the crystal growth is three-dimensional and controlled by interface reaction, the crystallisation rate $\frac{dx}{dt}$ is expressed as

$$\frac{dx}{dt} = (1-x) N 4\pi r^2 \frac{dr}{dt} \tag{7}$$

where N is the number of nuclei formed per unit volume, and x is the relative degree of crystallinity.
Taking the integration of Equation (7), the following equation is obtained.

$$-\ln(1-x) = \frac{4}{3}\pi N r^3 \tag{8}$$

For a heating process, the radius of a crystal particle r in Equation (8) can be replaced by Equation (6). It gives

$$-\ln(1-x) = \frac{4}{3}\pi N \left(\frac{U_0 E}{\beta R}\right)^3 \exp\left(-3\times 5.330 - 3\times 1.052\frac{E}{RT}\right) + \text{constant} \tag{9}$$

In a more generalised expression,

$$-\ln(1-x) = K_1 \beta^{-n} \exp\left(-1.052 m \frac{E}{RT}\right) + \text{constant} \tag{10}$$

Equation (10) can be rewritten as Equation (1) for estimating the activation energy for crystal growth. Since the crystallised fraction x at the peak temperatures T_p on DSC (or DTA) curves is almost constant irrespective of cooling rate β[5], Equation (2) is available at the peak temperature T_p. The activation energy can be calculated from the slope $-1.052 m E_g / nR$ provided that the numerical factors n and m are known.

However, for the case of crystallisation from the melt in a cooling process, the crystallisation commences from a high temperature. The relationship $|\Delta G| << RT$ cannot be met in this case. Therefore, Equation (2) cannot be simplified as Arrhenius form as Equation (3) under this condition. In addition, the radius r of crystal particle in this case can be expressed by the following equation

$$r = \int_{T_s}^{T} \frac{U}{\beta} dT = \frac{U_0}{\beta}\left[\int_0^T \exp(-E/RT)dT - \int_0^{T_s} \exp(-E/RT)dT\right] \quad (11)$$

where T_s is the starting temperature of the cooling process. Because T_s is larger than any certain temperature T during melt crystallisation, the value of the term $\int_0^{T_s} \exp(-E/RT)dT)$ in Equation (11) cannot be approximatively simplified as Equation (5).

It can be concluded when the crystallisation occurs from melt in a cooling process, the term $1-\exp(-\Delta G/RT)$ in basic rate equation of crystal growth and the term $\int_0^{T_s} \exp(-E/RT)dT$ depending on the starting temperature of the cooling process cannot be neglected. In this case, the radius r of crystal particle should be expressed as

$$r = \frac{U_0 \exp(-5.330)}{\beta R} \times \left\{ \begin{array}{l} \left[E\exp\left(-1.052\frac{E}{RT}\right) - E\exp\left(-1.052\frac{E+\Delta G}{RT}\right) - \Delta G\exp\left(-1.052\frac{E+\Delta G}{RT}\right)\right] \\ -\left[E\exp\left(-1.052\frac{E}{RT_s}\right) - E\exp\left(-1.052\frac{E+\Delta G}{RT_s}\right) - \Delta G\exp\left(-1.052\frac{E+\Delta G}{RT_s}\right)\right] \end{array} \right\} \quad (12)$$

Consequently, Equation (12) cannot be simplified as Equation (5), resulting in the failure in obtaining generalised expression Equation (2) for melts crystallisation based on the above derivation. Therefore, it can be concluded that the application of Equation (2) in determining activation energy for crystallisation that occurs on cooling is questionable.

The differential iso-conversional method of Friedman[20] and the advanced integral iso-conversional method of Vyazovkin[21] can be considered as alternatives to estimate activation energy for melts crystallisation. The Friedman equation is expressed as

$$\ln\left(\frac{dx}{dt}\right)_{x,i} = -\frac{E_x}{RT_{x,i}} + \text{constant} \quad (13)$$

where $T_{x,i}$ is the set of absolute temperatures related to a given relative degree of crystallinity at different cooling rates, and the subscript i is the ordinal number of individual cooling rate. Vyazovkin method has been designed to treat the kinetics that occur under arbitrary variation in temperature. For a series of n experiments carried out under different temperature programs, $T_i(t)$, the activation energy is determined at any particular value of relative degree of crystallinity x by finding E_x, which minimises the following function

$$\Phi(E_x) = \sum_{i=1}^{n}\sum_{j\neq i}^{n} \frac{J\left[E_x, T_i(t_x)\right]}{J\left[E_x, T_j(t_x)\right]} \quad (14)$$

Friedman equation and Vyazovkin equation have been extensively applied to evaluate the effective activation energy for non-isothermal melt crystallisation that occurs on cooling. The iso-conversional method of Friedman has been also successfully employed to determine the effective activation energy for non-isothermal crystallisation of lime-alumina-based mould fluxes that occurs on cooling in the authors' more recent study[22].

Melt crystallisation of $CaO-SiO_2-CaF_2$–based slags

Experimental

Reagent grade $CaCO_3$, SiO_2, CaF_2, Al_2O_3, MgO, and Na_2CO_3, were used as raw materials. The reagent powders were mixed well and melted in a platinum crucible with an induction furnace at 1300°C for 30 minutes to homogenise chemical composition, and then quenched into a cool steel plate to get fully glassy phase. The pre-melted samples were ground and analysed by X-ray fluoroscopy. The chemical compositions of pre-melted mould fluxes are shown in Table 1. The mould flux samples were crushed to prepare sample powder for DSC measurement. Differential Scanning Calorimetry (STA 449C; Netzsch Instrument Inc) measurement was performed under non-isothermal conditions at four different cooling rates (5, 10, 15, and 20 K/min) in Ar gas atmosphere. About 50 mg of sample powder was heated at a constant heating rate of 20 K/min from room temperature to 1300°C in a platinum crucible with a diameter of 5 mm and a height of 5 mm, and then held for 3 minutes to homogenise its chemical composition. Subsequently, the liquid sample was cooled to room temperature at constant cooling rates (5, 10, 15, and 20 K/min).

Table 1: Chemistry of investigated slags

Sample No.	Chemical Composition (wt%)						Basicity (CaO/SiO_2)
	CaO	SiO_2	MgO	Al_2O_3	Na_2O	F	
B	38.5 ± 0.3	41.1 ± 0.3	0.8 ± 0.5	5 ± 0.5	7.3 ± 0.5	7 ± 0.5	0.94
C	41.7 ± 0.3	36.7 ± 0.3	0.8 ± 0.5	5.3 ± 0.5	7.4 ± 0.5	7.2 ± 0.5	1.14
D	44.8 ± 0.3	33.4 ± 0.3	0.8 ± 0.5	5.4 ± 0.5	7.6 ± 0.5	7.6 ± 0.5	1.34

Non-isothermal crystallisation behaviours

In order to investigate the non-isothermal melt crystallisation, the heat released during crystallisation of mould fluxes has been measured by DSC. From these DSC curves, a few key parameters such as the crystallisation onset temperature T_{onset} and peak temperature T_{peak} can be obtained. Based on the assumption that the measured rate of released heat is proportional to the rate of crystallisation, the relative degree of crystallinity X(T) as a function of temperature can be formulated:

$$X_T = \frac{\int_{T_o}^{T} (dH_c / dT)dT}{\int_{T_o}^{T_f} (dH_c / dT)dT} \quad (15)$$

where T_o and T_f represent the onset and end crystallisation temperatures, respectively, and dHc/dT is the heat flow rate.

Considering the relationship between crystallisation time and temperature, the relative crystallinity can be converted to the function of time, using the following Equation (2).

$$t = \frac{T_O - T}{\beta} \quad (16)$$

where β is the cooling rate and T is the temperature at time t, T_o is temperature at which the crystallisation begins (t=0).

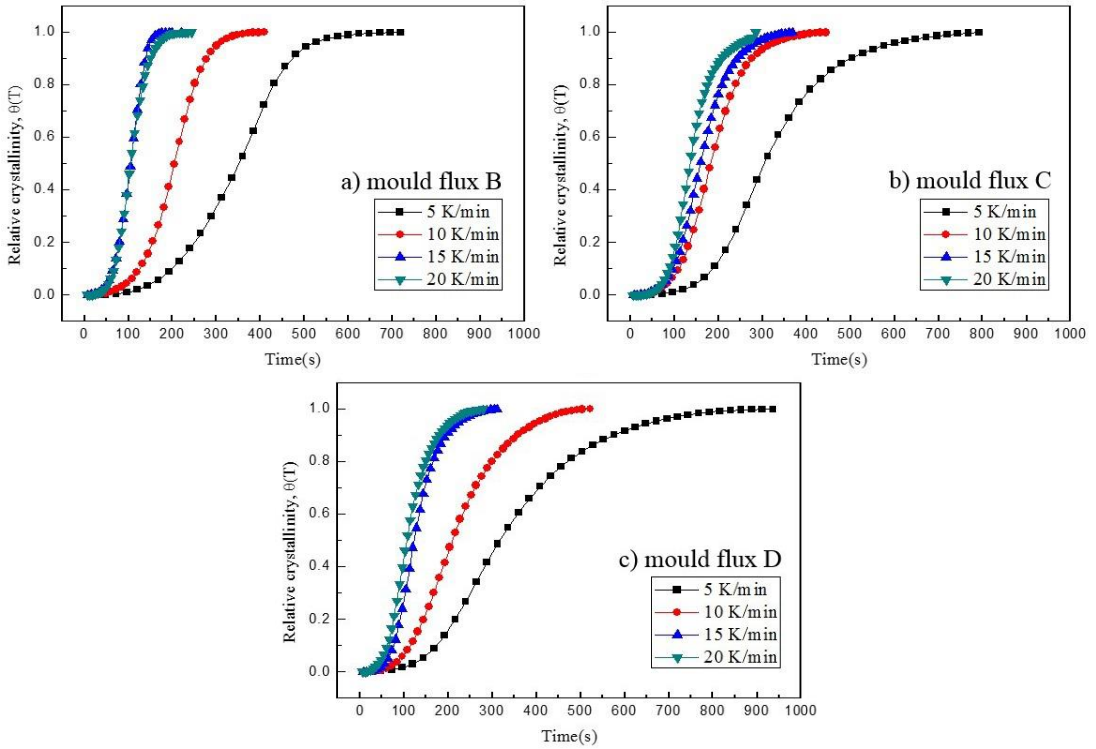

Figure 1: Relative crystallinity as a function of time of mould fluxes for four different cooling rates: (a) mould flux B, (b) mould flux C, (c) mould flux D

Figure 1 represents the relative degree of crystallinity as a function of time for investigated mould fluxes under four different cooling rates, 5 to 20 K/min. It is shown from Figure 1 that the time needed to complete crystallisation is in the range of 200-

400 sec for a cooling rate of 20 K/min, while it has been extended to 700-1000 sec for a cooling rate of 5 K/min. Crystallisation kinetics increase considerably with increasing the cooling rate from 5 K/min to 15 K/min, whereas this effect will be nearly saturated between 15 K/min and 20 K/min.

Effective activation energy for melt crystallisation

For non-isothermal crystallisation, kinetic analysis, various models[1-4] have been proposed to determine the activation energy. Among them, the Kissinger[1] and Matusita[4] equations are most frequently used to determine the activation energy for the crystallisation that occurs on heating[8,9]. On cooling, the temperature decreases with the time, resulting in negative value of dT/dt. However, it should be emphasised that the Kissinger and Matusita equations does not permit substitution of negative value of dT/dt. This problem has been bypassed by dropping off the minus sign. Vyazovkin[21,23] clarified that these methods provided invalid results when it was applied to melt crystallisation that occurred on cooling process. The problem of negative dT/dt can be avoided by applying the iso-conversional methods which are recommended by Brown *et al.*[24]. Iso-conversional methods can be applied to melt crystallisation that occurred on cooling for evaluating the dependence of the effective activation energy on conversion. These methods could be helpful in revealing complex crystallisation kinetics which is composed of nucleation and crystal growth having multiple Arrhenius equation. Among them, the differential iso-conversional method developed by Friedman[20] was employed to determine the effective activation energy for the crystallisation of cuspidine phase in the present work.

According to the Friedman equation, the effective activation energy is obtained at a given degree of crystallinity and expressed as follows:

$$\ln\left(\frac{dX}{dt}\right)_X = -\frac{\Delta E_X}{RT_X} + C \tag{17}$$

where ΔE_X is the effective activation energy at a given relative degree of crystallinity X, T_X is the temperature corresponding to a given X at different cooling rate. The instantaneous crystallisation rate dT/dt can be determined from experimentally measured DSC data using the following equation.

$$\frac{dX}{dt} = \frac{dH_c / dt}{\int_{t_0}^{t_f} \left(dH_c / dt\right) dt} \tag{18}$$

where dH_c represents the measured enthalpy of crystallisation during time interval, t_0 is the time at which the crystallisation begins, and t_f is the time at which the crystallisation is completed.

The values ΔE_X of are associated with the temperatures at a given relative crystallinity X. By plotting ln(dX/dt) versus $1/T_x$ at different relative crystallinity X, a straight line should be obtained. From the slope of straight line, the effective activation energy ΔE_X at different relative degree of crystallinity X can be determined.

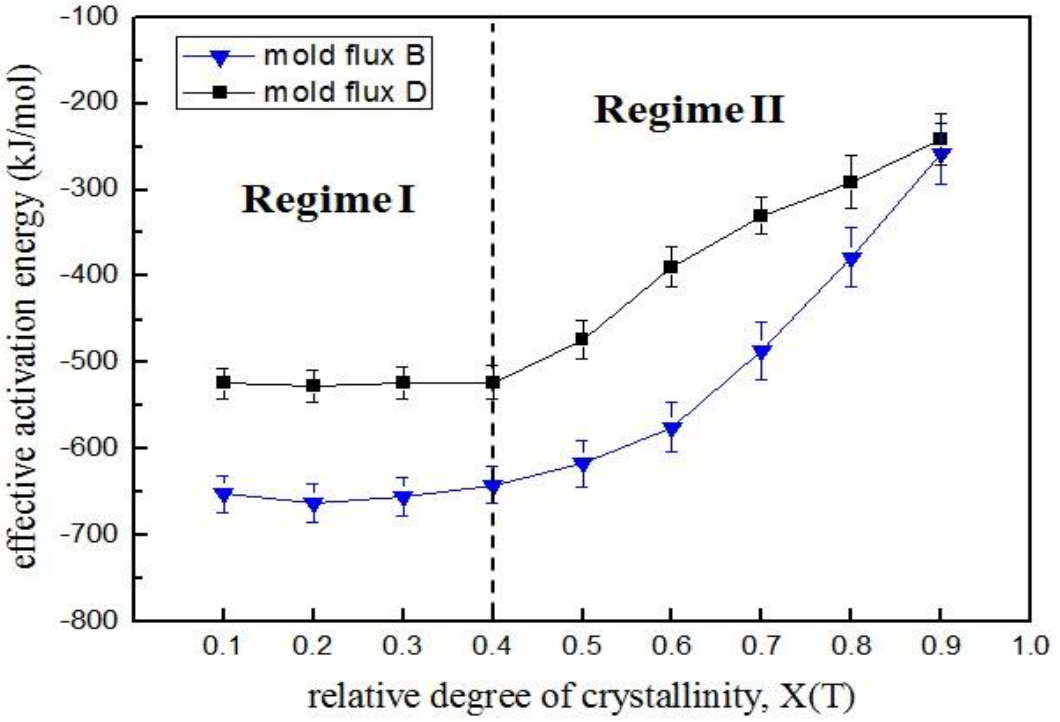

Figure 2: Dependence of the effective activation energy on the relative degree of crystallinity in non-isothermal crystallisation of mould flux B and D

Figure 2 shows the dependence of the effective activation energy on the relative extent of crystallinity in non-isothermal crystallisation of mould flux B and D. It is obvious that the change in the dependence of the effective activation energy for both mould fluxes is similar, implying that crystallisation of mould flux B and D is governed by the same mechanism. The dependence of effective activation energy on the relative extent of crystallinity could indicate the temperature dependence of crystallisation rate because the crystallisation is a complex process governed by nucleation and crystal growth, which involves temperature-dependent steps and one of them determines the overall crystallisation rate. As shown in Figure 2, the effective activation energy for both mould fluxes remains constant over the range from 0.1 to 0.4, whereas it increases as the extent of crystallinity rises. From this result, one can find that the rate controlling step for the cuspidine crystallisation should be complex: nucleation and/or crystal growth. The change in the shape of the dependence of the effective activation energy is closely associated with the nucleation behaviour during non-isothermal cooling. Based on the classical nucleation theory[25], the temperature dependence of the nucleation rate can be expressed as follows

$$\dot{N} = n_o \exp\left(\frac{-E}{RT}\right)\exp\left(\frac{-\Delta G^*}{RT}\right) \quad (19)$$

where $\dot{N}$ is the nucleation rate, n_0 is pre-exponential factor, and ΔG^* is free energy terms for nucleus formation. Here, it is known that free energy term is inversely proportional to the degree of undercooling and is given by following Equation (20)[26].

$$\Delta G^* \approx \frac{1}{(T_m - T)^2} \quad (20)$$

where T_m is the melting point of mould fluxes, and T_m-T represents the degree of undercooling.

It can be seen from Figure 2 that the effective activation energy for both mould fluxes has the greatest negative values at lower degree of crystallinity. It is interestingly noticed that the value of ΔG* can be very large adjacent to melting temperature of the molten mould fluxes, giving rise to the fact that the initial crystallisation rate is governed by the nucleation rate. It is noted from Equation (8) that ΔG* decreases with decreasing temperature, indicating that the nucleation rate increases by cooling. In regime I in Figure 2, therefore, the crystallisation behaviour should be determined by the thermodynamic term of nucleation relating to free energy change for nucleus formation. Above the relative crystallinity degree of 0.4, as can be seen in Figure 2, the effective activation energy for both mould fluxes increases as crystallisation progresses. In regime II in Figure 2, the crystallisation behaviour should be governed simultaneously by nucleation and crystal growth. These phenomena are well represented in Figure 3 which shows schematics of crystallisation rate as function of nucleation and crystal growth rate. It should be stressed that values of effective activation energy in both mould fluxes are negative, indicating that the crystallisation of cuspidine on cooling process obeys an anti-Arrhenius behaviour. A similar behaviour on the dependence of effective activation energy has already been reported by Vyazovkin *et al.*[24] and Papageorgiou *et al.*[27] for the crystallisation of polymers.

It is observed from Figure 2, that effective activation energy for mould flux D was lower than that of mould flux B, which reveals that the crystallisation for mould flux B requires more undercooling to crystallise. The undercooling of mould flux B and D for cuspidine formation is 60.2 K and 9.6 K, respectively. The difference of undercooling degree could lead to the difference of crystal morphology. As thermodynamic term of nucleation is inversely proportional to undercooling degree, nucleation rate for mould flux B should be much larger than that for mould flux D. This finding can be confirmed by the crystal morphology as shown in Figure 4.

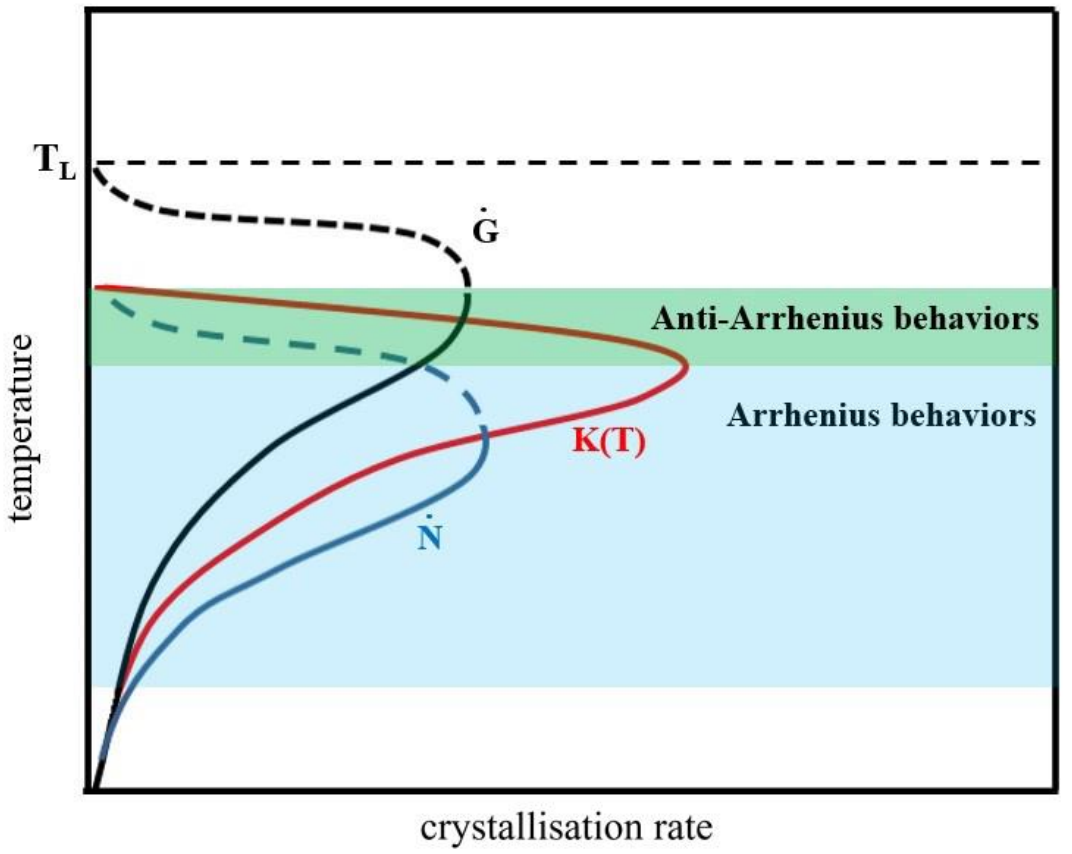

Figure 3: Schematic diagram of crystallisation rate, K(T) as function of nucleation (N) and crystal growth rate (G): the green region follows Anti-Arrhenius behaviours, whereas the blue region obeys Arrhenius behaviours. (dotted lines for thermodynamic controlled region, solid lines for kinetic controlled region for both growth and nucleation rate)

Crystal morphology

Figure 4 shows BSE images of mould flux B and D after DSC measurement at the cooling rate of 20 K/min. For mould flux B, the crystal morphology is largely dendritic, which is composed of many nuclei as shown in Figure 4a. On the other hand, in the mould flux D, the crystal morphology is mainly faceted as shown in Figure 4b. This finding is consistent with other studies[28-33] which reported that the morphology of crystals is mainly faceted at lower undercooling, whereas the morphology of crystals is mainly dendritic at higher undercooling. This phenomenon can be explained by interface stability theory[31]. At higher undercooling, the faceted interfaces become unstable and change into dendritic crystals[32,33].

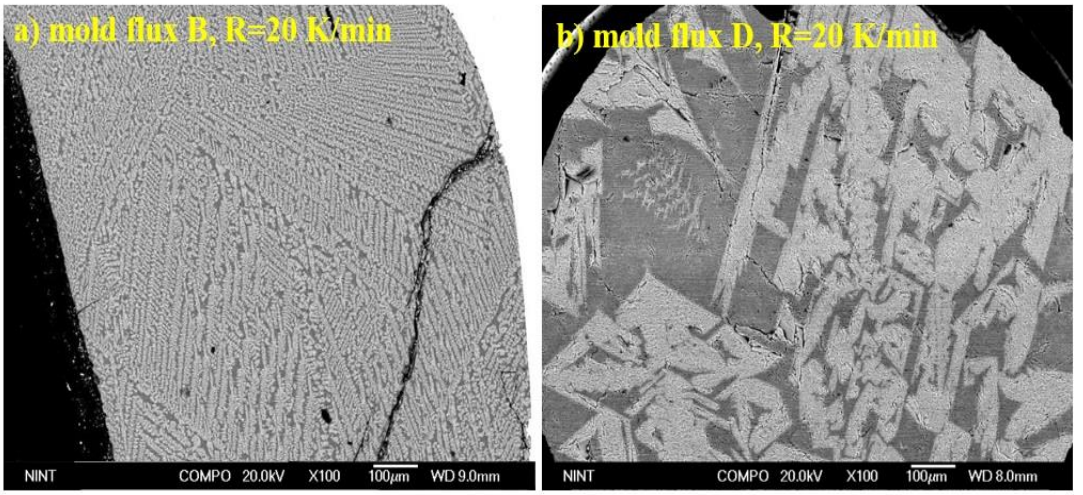

Figure 4: BSE images of mould fluxes after DSC measurement at the cooling rate of 20 K/min: (a) mould flux B, (b) mould flux D

It can be observed from Figure 4a and 4b that the size of cuspidine increases with increasing the mould flux basicity. This is due to an increase in crystallisation temperature with increasing mould flux basicity, giving rise to the increase of mass transfer in a melt for the cuspidine growth.

Controlling the crystal morphology

Jackson suggested a system in which the solid and liquid phases were separated by an interface with one-layer atom thickness, and he calculated the surface free energy changes as a function of the ratio of site occupancy of the constituent unit on the interface, as shown in Equation (21).

$$\frac{\Delta F}{NkT} = X(1-X)\alpha + X\ln X + (1-X)\ln(1-X) \tag{21}$$

where ΔF is the change in surface free energy, N is the number of the crystal surface lattice sites, k is the Boltzmann's constant, T is the absolute temperature and X is fraction of surface sites occupied, respectively. Also, α is the so-called Jackson roughing factor that is defined as Equation (22). As can be obtained from Equation (21), for materials with α < 2, there is only one minimum value at 50% of surface site occupancy, indicating that the interface energetically prefers to be rough. On the other hand, in a material with α > 3, there are two energy minima at site occupancy 0 and 100%, suggesting that the interface will be smooth on the atomic scale and the corresponding crystal turns out faceted in morphology.

$$\alpha = \xi_{(hkl)} \frac{\Delta H_m}{RT} \tag{22}$$

In Equation (22), ΔH_m is the enthalpy change for the crystal dissolution into melt bulk, which could be calculated with the help of thermodynamic database such FactSage; R is the ideal gas constant; $\xi_{(hkl)}$ is the orientation factor, defined as the ratio between nearest sites for a growth unit in the surface of a crystal and the coordination number.

Jackson proposed α factor to evaluate the crystal morphology only on the basis of a thermodynamic equilibrium system. In the non-equilibrium melt, the driving force, such as the thermal supercooling or constitutional supercooling, also affects the crystalline morphology and it is so called kinetic roughening[34,35]. The driving force for a crystal nucleation and growth to take place is the degree of departure from the equilibrium state. In melt crystallisation, the driving force can be evaluated as the difference between the equilibrium melting point and growth temperatures,

$$\Delta T = T_m - T \quad \text{(supercooling)} \tag{23}$$

To compare the supercooling among different melts, the supercooling degree is also used in the present article, defined as $\Delta T / T_m$.

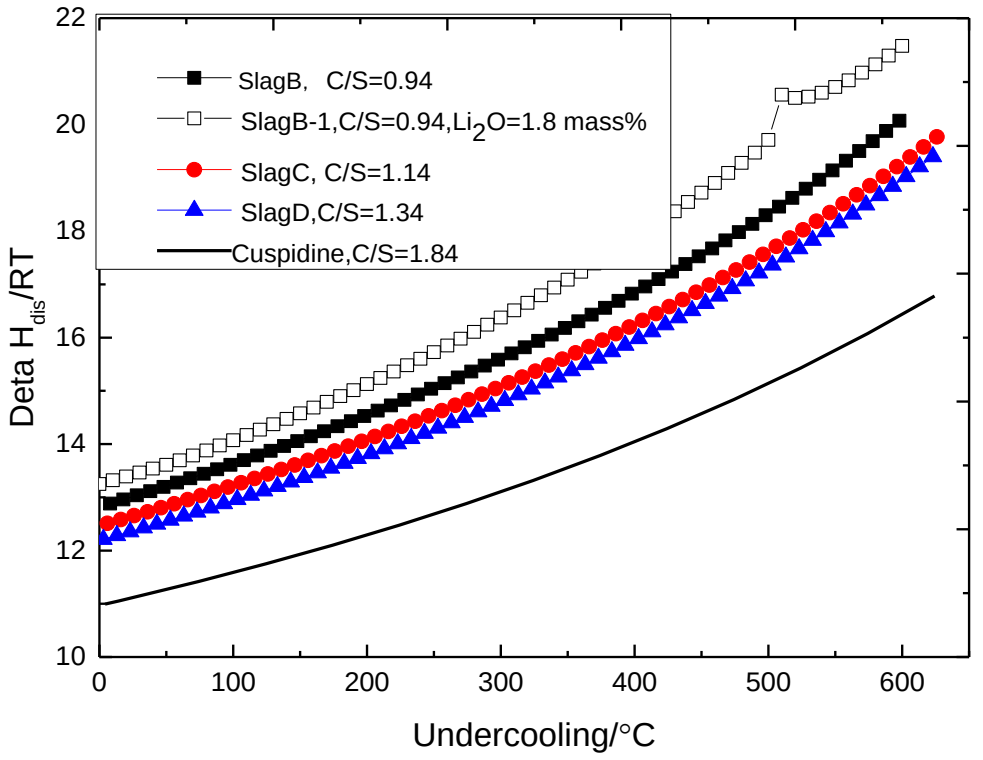

Figure 5: Jackson α factor for cuspidine precipitation in four kinds of $CaO\text{-}SiO_2$-based mould fluxes under different supercooling

Figure 5 shows the calculated Jackson factors for cuspidine in the four types of lime-silica based mould fluxes including the pure cuspidine melt, *i.e.*, with same stoichiometric composition as cuspidine. It can be seen that the Jackson α factor of

cuspidine crystal increase slightly with the mould flux basicity decrease by comparing that of Slag B, C and D and increases with a small amount of Li_2O addition by comparing Slag B-1 and B. In addition, it increases with the supercooling increase. Figure 6 shows the supercooling degree and their corresponding Jackson factors for the cuspidine crystallisation in the four kinds of lime-silica based mould fluxes, where the y axis is drawn as the degree of supercooling degree ($\Delta T / T_m$) for a fairer comparison. Similar to Temkin's[34,35] conclusion, a critical line for cuspidine crystal kinetic roughening can be evaluated as well, shown as the dot line in the Figure. When the supercooling is lower than the critical line (Region A), the cuspidine morphology is faceted, whereas the crystal morphology appears dendritic shape when the supercooling over the critical value (Region B) as the kinetic roughening occurs. For the cuspidine precipitation from these lime-silica based mould fluxes, the critical degree of supercooling is estimated between 0.05-0.06 and increases with the Jackson α factor.

According to Figures 5 and 6, ones know that the supercooling has complicated effects on the cuspidine morphology: by increasing supercooling within the critical line region, it will increase the Jackson α factor and, thus, enhance faceted cuspidine precipitation; while supercooling over the critical value, kinetic roughening takes place and it is likely to precipitate dendritic cuspidine. The supercooling for crystallisation of the slag B is remarkably larger than that of slag D, thus crystal in the slag B is more likely to be dendritic. Interestingly, the present findings are in quite good agreement with Lu *et al.*'s[36] and Heulens'[37] experimental results regarding the alpha Ni crystal and wollastonite morphology evolution under different supercooling. By combining the present results with Temkin's, it can be concluded that the crystal with higher Jackson factor is more difficult to form dendritic structure as greater critical supercooling degree is usually needed. Also, it shows the similar tendency in lime-alumina based mould fluxes, some CaF_2 crystal is dendritic under the relative low supercooling (< 50°C) due to its small Jackson α factor value, while the calcium aluminate and calcium borate crystals remain faceted morphology under relative high supercooling (100-200°C due to their relative larger Jackson α factor. Practically, one could control faceted or dendritic crystal morphology by matching the suitable Jackson α factor in the manner of the melt composition adjustment and heat treatment on the basis of the similar crystal morphology transition diagram like Figure 6, thus these kinds of diagrams are very essential for crystal morphology control.

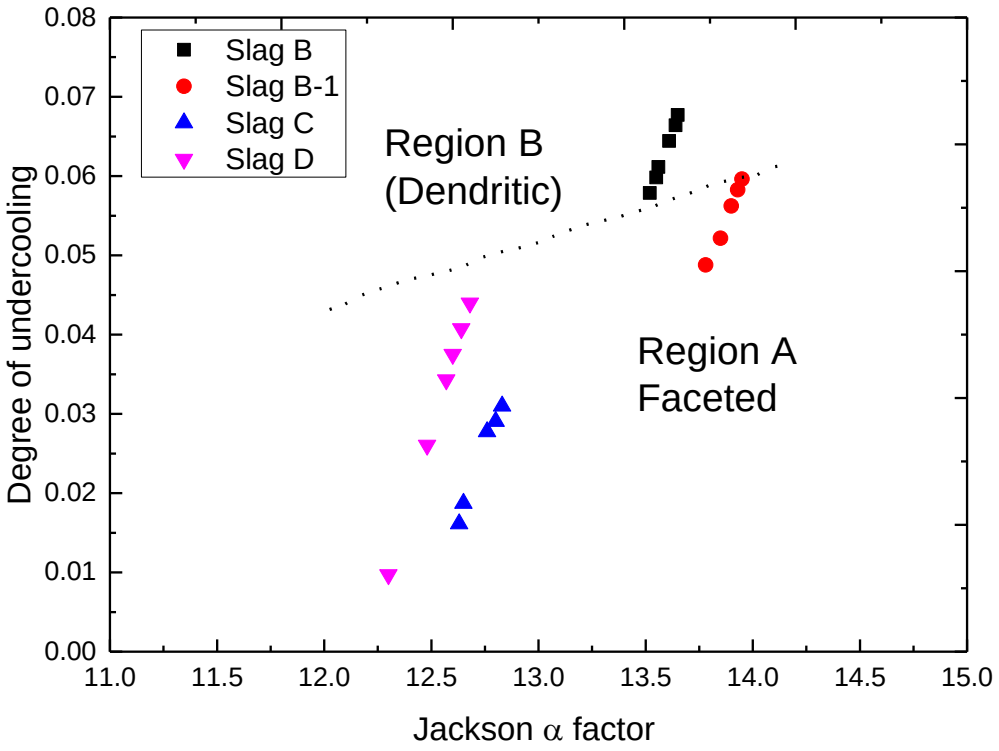

Figure 6: Degree of undercooling and Jackson α factor dependence of cuspidine crystal morphology

Conclusions

1. Matusita equation is inapplicable to estimate the activation energy associated with the melt crystallisation that occurs on cooling. The iso-conversional methods of Friedman and Vyazovkin are recommended to determine effective activation energy for melts crystallisation that occurs on cooling.

2. The dependence of effective activation energy on the relative extent of crystallinity during non-isothermal crystallisation was estimated by applying differential iso-conversional method of Friedman analysis. The obtained effective activation energy for the glasses ranges from -241 to -652 kJ/mol. The negative signs of effective activation energy mean the anti-Arrhenius kinetics during melt crystallisation, giving rise to the fact that mould fluxes crystallisation for the cuspidine formation is determined by thermodynamic term of nucleation which is related to undercooling degree.

3. The morphology of cuspidine crystals for the glass with largest basicity, 1.34, is mainly faceted at lower undercooling, whereas the morphology of cuspidine crystals for smallest basicity, 0.94, is mainly dendritic at higher undercooling. This supported the anti-Arrhenius behaviour for melt crystallisation kinetics of the glasses investigated.

4. Jackson α factor was introduced to understand the crystal morphology control in a multi-component mould flux. In addition, the enthalpy of dissolution and the corresponding Jackson α factors for crystals of melt crystallisation in multi-component mould flux were established and reasonably evaluated by applying the thermodynamic database such as FactSage.

References

1. H. E. Kissinger, "Reaction kinetics in differential thermal analysis", *Anal Chem*, **29** 1702-1706 (1957).
2. T. Ozawa, "Kinetic analysis of derivative curves in thermal analysis", *J Therm Anal*, **2** 301-324 (1970).
3. H. S. Chen, "A method for evaluating viscosities of metallic glasses from the rates of thermal transformations", *J Non-Cryst Solids*, **27** 257-263 (1978).
4. K. Matusita and S. Sakka, "Kinetic study of crystallization of glass by differential thermal analysis-criterion on application of Kissinger plot", *J Non-Cryst Solids*, **38-39** 741-746 (1980).
5. K. Matusita, T. Komatsu and R. Yokota, "Kinetics of non-isothermal crystallization process and activation energy for crystal growth in amorphous materials", *J Mater Sci*, **19** 291–296 (1984).
6. C. T. Cheng, M. Lanaganw, B. Jones, J. T. Lin and M. J. Pan, "Crystallization Kinetics and Phase Development of PbO–BaO–SrO–Nb2O5–B2O3–SiO2-Based Glass–Ceramics", *J Am Ceram Soc*, **88** 3037–3042 (2005).
7. B. Rangarajan, T. Shrout and M. Lanagan, "Crystallization kinetics and dielectric properties of fresnoite BaO - TiO2 - SiO2 glass – ceramics", *J Am Ceram Soc*, **92** 2642–2647 (2009).
8. S. R. Teixeiraw, M. Romero and J. M. Rincón, "Crystallization of SiO2-CaO-Na2O Glass Using Sugarcane Bagasse Ash as Silica Source", *J Am Ceram Soc*, **93** 450-455 (2010).
9. M. Romero, J. Martíin-Márquez and J. M. Rincón, "Kinetic of mullite formation from a porcelain stoneware body for tiles production", *J Eur Ceram Soc*, **26** 1647-1652 (2006).
10. Z. Wang, Q. Shu and K. Chou, "Crystallization Kinetics and Structure of Mold Fluxes with SiO2 Being Substituted by TiO2 for Casting of Titanium-Stabilized Stainless Steel", *Metall Mater Trans B*, **44B** 606–613 (2013).
11. M. Joshi and B. S. Butola, "Studies on non-isothermal crystallization of HDPE/POSS Nanocomposites", *Polym*, **45** 4953-4968 (2004).
12. S. H. Kim, S. H. Ahn and T. Hirai, "Crystallization kinetics and nucleation activity of silica nanoparticle-filled poly(ethylene 2,6-naphthalate)", *Polym*, **44** 5625-5634 (2003).
13. T. Liu, Z. Mo, S. Wang and H. Zhang, "Non-isothermal melt and cold crystallization kinetics of poly(aryl ether ether ketone ketone)", *Polym Eng Sci*, **37** 568-575 (1997).
14. K. Y. Mya, K. P. Pramoda and C. B. He, "Crystallization behavior of star-shaped poly(ethylene oxide) with cubic silsesquioxane (CSSQ) core", *Polym*, **47** 5035–5043 (2006).
15. S. Zhao, Z. Cai and Z. Xin, "A highly active novel β-nucleating agent for isotactic polypropylene", *Polym*, **49** 2745–2754 (2008).
16. S. Y. Choi, D. H. Lee, D. W. Shin, S. Y Choi, J. W. Cho and J. M. Park, "Properties of F-free glass system as a mold flux: viscosity, thermal conductivity and crystallization behaviour", *J Non-Cryst Solids*, **345-346** 157-160 (2004).
17. L. Gan, C. X. Zhang, J. C. Zhou and F. Q. Shangguan, "Continuous cooling crystallization kinetics of a molten blast furnace slag", *J Non-Cryst Solids*, **358** 20-24 (2012).
18. K. Matusita, K. Miura and T. Komatsu, "Kinetics of non-isothermal crystallization of some fluorozirconate glasses", *Thermochim Acta*, **88** 283-288 (1985).
19. C. D. Doyle, "Kinetic analysis of thermogravimetric data", *J Appl Polym Si*, **5** 285-292 (1961).

20. H. L. Friedman, “Kinetics of thermal degradation of char-forming plastics from thermogravimetry: Application to a phenolic plastic”, *J Polym Sci Part C*, **6** 183-195 (1964).
21. S. Vyazovkin, “Is the Kissinger Equation Applicable to the Processes that occur on Cooling?”, *Macromol Rapid Commun*, **23** 771-775 (2002).
22. C. B. Shi, M. D. Seo, H. Wang, J. W. Cho and S. H. Kim, “Evaluation of Matusita Equation and Its Modified Expression for Determining Activation Energy Associated with Melt Crystallization”, *Metall Mater Trans B*, **45B** 1987-1991 (2014).
23. S. Vyazovkin and N. Sbirrazzuol, “Iso-conversional Analysis of Calorimetric Data on Nonisothermal Crystallization of a Polymer Melt”, *J Phys Chem*, **107** 882-888 (2003).
24. M. E. Brown, M. Maciejewski, S. Vyazovkin, R. Nomen, J. Sempere, A. Burnham, J. Opfermann, R. Strey, H. L. Anderson, A. Kemmler, R. Keuleers, J. Janssens, H. O. Desseyn, C. R. Li, T. B. Tang, B. Roduit, J. Malek and T. Mitsuhashi, “The ICTAC kinetics project-data, methods and results”, *Thermochim Acta*, **355** 125-143 (2000).
25. D. Turnbull and J. C. Fisher, “Rate of Nucleation in Condensed Systems”, *Chem Phys*, **17** 71 (1949).
26. J. M. Schultz, *Polymer Material Science*, Prentice Hall, Englewood (1974).
27. G. Z. Papageorgiou, D. S. Achilias, D. N. Bikiaris and G. P. Karayannidis, “Crystallization kinetics and nucleation activity of filler in polypropylene/surface-treated SiO2 nanocomposites”, *Thermochim Acta*, **427** 117-128 (2005).
28. S. S. Jung and I. Sohn, “Crystallization Behavior of the CaO-Al2O3-MgO System Studied with a Confocal Laser Scanning Microscope”, *Metall Mater Trans B* **43** 1530-1539 (2012).
29. C. Orrling, S. Sridhar and A. W. Cramb, “In situ observation of the role of alumina particles on the crystallization behavior of slags”, *ISIJ Int*, **40** 877-885 (2000).
30. J. Li, W. Wang, J. Wei, D. Huang and H. Matsuura, “A kinetic Study of the Effect of Na2O on the Crystallization Behavior of Mold Fluxes for Casting Medium Carbon Steel”, *ISIJ Int*, **52** 2220-2225 (2012).
31. R. J. Kirkpatrick, “Crystal-growth from melt-review”, *Am Mineral*, **60** 798-814 (1975).
32. J. Huelens, B. Blanpain and N. Moelans, “Analysis of the isothermal crystallization of CaSiO3 in a CaO-Al2O3-SiO2 melt through in situ observation”, *J Eur Ceram Soc*, **31** 1873-1879 (2011).
33. D. Li and D. M. Herlach, “Direct Measurements of Free Crystal Growth in Deeply Undercooled Melts of Semiconducting Materials”, *Phys Rev Lett*, **77** 1801-1804 (1996).
34. O. E. Temkin, “Phenomenological kinetics of the motion of a phase boundary”, *Sov Phys Cryst*, **15** 767-772 (1971).
35. O. E. Temkin, “Kinetic phase transition during a phase conversion in a binary alloy”, *Sov Phys Cryst*, **15** 773-780 (1971).
36. Y. Lu, G. Yang, F. Liu, H. Wang and Y. Zhou, “The transition of alpha-Ni phase morphology in highly undercooled eutectic Ni78.6Si21.4 alloy”, *Europhys Lett*, **74** 281-286 (2006).
37. J. Heulens, B. Blanpain and N. Moelans, “Analysis of the isothermal crystallization of CaSiO3 in a CaO–Al2O3–SiO2 melt through in situ observations”, *J Eur Ceram Soc*, **31** 1873-1879 (2011).